ACS APPLIED MATERIALS & INTERFACES

Research Article

www.acsami.org

Novel, Facile, Single-Step Technique of Polymer/TiO_2 Nanofiber Composites Membrane for Photodegradation of Methylene Blue

Abdalla Abdal-hay,*[,†,‡] Abdel Salam Hamdy Makhlouf,*[,§] and Khalil Abdelrazek Khalil[∥,⊥]

[†]Department of Engineering Materials and Mechanical Design, Faculty of Engineering, South Valley of University, Qena 83523, Egypt

[‡]Department of Bionano System Engineering, College of Engineering, Chonbuk National University, Jeonju 561-756, Republic of Korea

[§]Department of Manufacturing Engineering, College of Engineering and Computer Science, University of Texas Pan-American, 1201 West University Drive, Edinburg, Texas 78541-2999, United States

[∥]Department of Mechanical Engineering, College of Engineering, King Saud University, Riyadh 11421, Saudi Arabia

[⊥]Department of Mechanical Engineering, Faculty of Energy Engineering, Aswan University, Aswan, Egypt

Supporting Information

ABSTRACT: Novel photocatalyst membrane materials were successfully fabricated by an air jet spinning (AJS) technique from polyvinyl acetate (PVAc) solutions containing nanoparticles (NPs) of titanium dioxide (TiO_2). Our innovative strategy for the production of composite nanofibers is based on stretching a solution of polymer with a high-speed compressed air jet. This enabled us to rapidly cover different substrates with TiO_2/PVAc interconnected nanofibers. Surprisingly, the diameters of the as-spun fibers were found to decrease with increasing amount of NPs. Our results showed that AJS PVAc-based fibrous membranes with average fiber diameters of 505−901 nm have an apparent porosity of about 79−93% and a mean pore size of 1.58−5.12 μm. Embedding NPs onto the as-spun fibers resulted in increasing the tensile strength of the obtained composite fiber mats. The photodegradation property of TiO_2 membrane mats proved a high efficiency in the decomposition of methylene blue dye. The novel fiber spinning technique discussed in this paper can provide the capacity to lace together a variety of types of polymers, fibers and particles to produce interconnected fibers layer. Our approach, therefore, opens the door for the innovation in nanocomposite mat that has great potential as efficient and economic water filter media and as reusable photocatalyst.

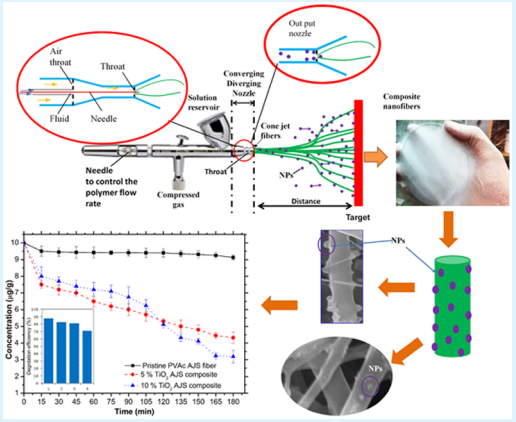

KEYWORDS: *water treatment, nanofilter, nanocomposite membrane, polymer/TiO_2nanofibers*

1. INTRODUCTION

Photocatalysis has been demonstrated as a low cost and sustainable technology for the treatment of pollutants in air and water including organics and heavy metals.[1,2] Titanium dioxide (TiO_2) is the most frequently used photocatalyst because of its photostability, low cost, and resistance to corrosion.[3−7] Additionally, TiO_2 nanoparticles (NPs) have high capability to absorb ultraviolet and pigments and which allows it to be used for photocatalytic degradation of pollutants in water. Therefore, TiO_2 NPs are widely used as effective and stable photocatalysts for water pollutants. Unfortunately, most of the researchers ignored the separation process of the utilized TiO_2 NPs from the treated water. This created a secondary pollution problem where the free TiO_2 NPs that remain in the environment have been shown to be harmful to living organisms.[8] Besides, the tendency of the NPs to agglomerate into larger particles can result in a reduction of the photocatalytic efficiency during the cycling use,[9,10] which is another dilemma in water treatment.

To avoid free NPs in water, TiO_2 NPs are usually immobilized on a substrate or integrated into thin-films or polymers. In these regards, polymer materials substrates play an important role in immobilizing active catalyst[11−13] because of their good film forming ability, flexibility, toughness, separation properties, and cost-effective.

Different methods have been used to incorporate inorganic NPs into a polymer matrix. Electrospinning is the most existing popular strategy used for production of polymer and composite nanofibers mats that contain high-quality nanofibers.[14] Electrospinning can be performed by charging a droplet of polymer liquid using electricity. Despite the versatility of electrospinning technique, there are still several drawbacks that limit its application in industry. Examples of these drawbacks are the need for a high-voltage power supply, the sensitivity to the

Received: February 23, 2015
Accepted: May 18, 2015
Published: May 18, 2015

DOI: 10.1021/acsami.5b01418
ACS Appl. Mater. Interfaces 2015, 7, 13329−13341

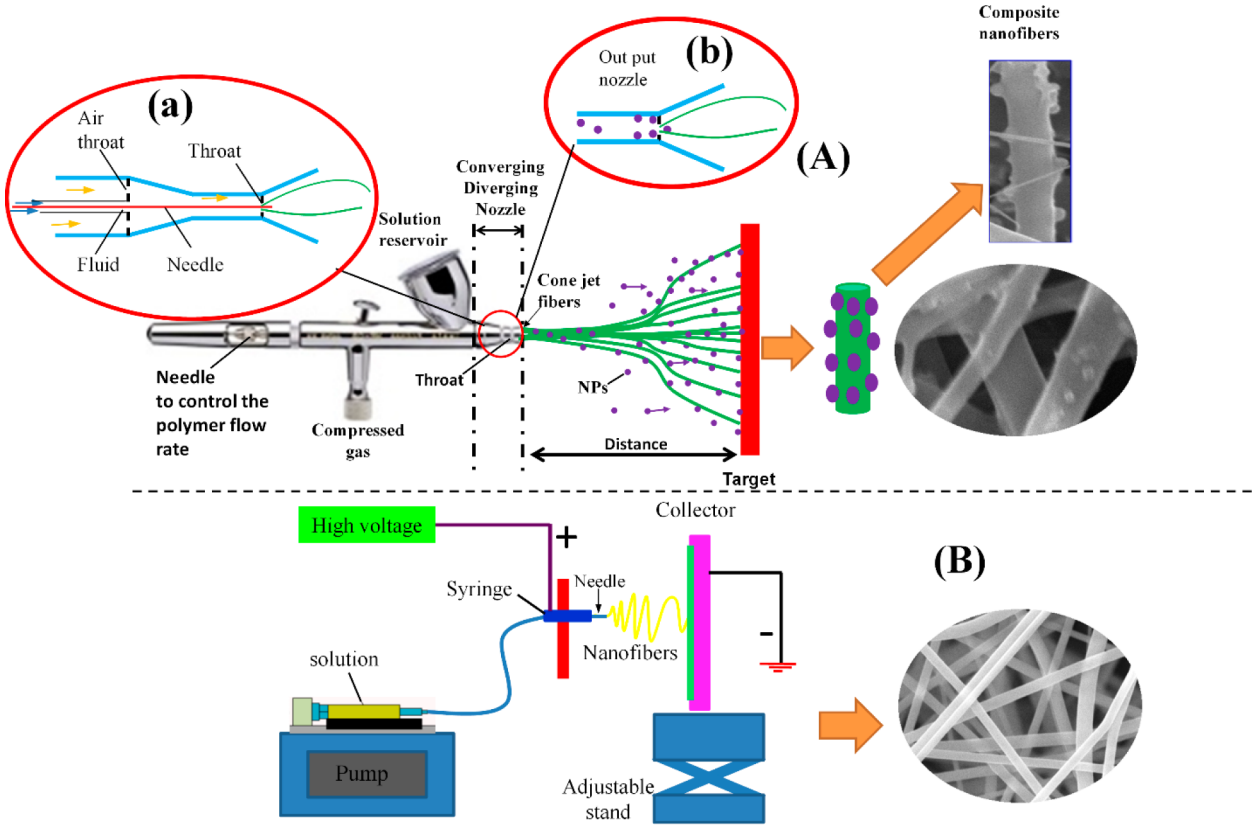

Figure 1. Comparison of the air jet (A) spinning and (B) electrospinning approaches for fabricating nanofiber membrane mats. Insets a and b of panel A illustrate convergent-divergent nozzle and output throat of AJS mechanism.

change in solution conductivity, very low production rate (0.3 g/h per jet), and the difficulty to fabricate 3D open structures.[14]

Several researchers have attempted to find an alternative method for fabrication of 3D porous nanofibers suitable for several applications. For example, Benavides and co-workers have fabricated micronano scale fibers based on high velocity expanding gas jet.[14] However, this process seems quite complex and hard to fellow due to applying multi necessary steps to obtain nanofibers. Recently, our research group has successfully developed a novel, simple and cost-effective one-step air jet spinning (AJS) system for fabrication of 3-D porous and micronano polymeric fibers.[15−17] AJS is a simple processing technique that allows fabrication of high aspect ratio nanofibers in a commercial scale. A number of advantages including low capital cost, lower energy requirements, high fibers production rate and ease of operation can be offered by the AJS. Our system is based on exploiting a high-speed compressed air onto the prepared solution to form a polymer jet, which undergoes extensive stretching before solidification (Figure 1A). On the basis of our previous results, TiO_2 NPs can be immobilized onto individual fiber surface during the fabrication process using the same principle of AJS. Thus, the catalytic capability can be enhanced using an AJS nanofiber mat as catalyst carrier (the extremely large surface due to the nanofiber structure can provide a huge number of active sites). Accordingly, we expect that this technique can enable the surfaces to be covered very rapidly with a nonwoven polymer composite fiber matrix.

The rubbery polymers can perfectly adhere to variable surfaces owing to their soft and flexible nature.[17] Therefore, we have chosen polyvinyl acetate (PVAc) as a polymer matrix to immobilize inorganic TiO_2 NPs for photocatalytic applications. PVAc is expected to avoid the problems associated with the use of soft and rigid polymers. PVAc is commonly used as an adhesive, binder, coating and a biomedical material.[18,19] Results showed that PVAc has good adhesion with the inorganic fillers. Our previous results showed that PVAc could induce a superior fiber formatting capability using the AJS technique and has a superior adhesion performance on metal substrates.[17,20]

Herein, novel composite photocatalysts nanofiber membrane (CPNM) composed of an adhesive polymer (as a fiber continuous phase) and loaded with TiO_2 NPs (as a dispersed phase) were prepared and characterized. To the best of our knowledge, this pair of polymer and filler has never been used before in the literature to prepare CPNM matrix by means of AJS. The combination of PVAc and TiO_2 employing AJS for making CPNM can cause Ti−OH groups on the surface of TiO_2 to react with the alkyl group hydrogen of the PVAc chain, making hydrogen bonding at the interface before and upon impact of AJS fluctuated NPs onto fiber substrates. In this way, TiO_2 NPs may be anchored to the fiber surface of PVAc molecules such that the surface of individual fiber will be decorated with the NPs. Consequently, mixing of these two materials at the nanoscale and then applying them as a coating using AJS technique proved to provide superior adhesion and tensile properties in addition to the formation of a unique and effective multifunctional CPNM. Formation of multifunctional CPNM can lead to a remarkable increase in the number of reactive sites with a corresponding improvement in hydrophilicity and photocatalytic activity in the oxidation of dyes. Also, we were able to coat high-aspect-ratio polymeric nanofiber mats with TiO_2 NPs without aggregation by means of AJS. The morphologies of membrane surfaces porosity, pore

DOI: 10.1021/acsami.5b01418
ACS Appl. Mater. Interfaces 2015, 7, 13329−13341

size and pore size distribution were studied. The interactions between nano-TiO_2 particles and PVAc polymer were analyzed by XRD and FTIR methods. This CPNM matrix prepared by AJS can play an important role in immobilizing active catalyst and would have a great potential for pollutant removable sources applications, such as water treatment, especially in the developing countries, where millions of people die each year because of polluted drinking water.

2. EXPERIMENTAL SECTION

2.1. Raw Materials. Polyvinyl acetate was supplied from Sigma-Aldrich with an average M_w of 500 000 and viscosity 60.0−75.0 cps. It was provided in the bead shape and hydrophobic nature. Dichloromethane (CH_2Cl_2, DCM) was purchased from Junsei Chemical Co., Japan in spectrophotometer grade 99.5% pure, having density 1.325 g/cm^3 at 25 °C, boiling point 40 °C. The low boiling point of DCM ensure that it will need relatively shorter time to evaporate and subsequently ease the formation of micronano scale fibers using AJS strategy. In addition, it helps to avoid sedimentation of the inorganic particles in the resulting nanocomposites membrane. TiO_2 powder, 99.8% trace metals basis, was supplied from Sigma-Aldrich. The powder particle size was in a range of 60−230 nm (morphological properties using FESEM TiO_2 particles used in this study are shown in the Supporting Information, Figure S1). From the image, it is a heterogeneous material containing small spheres.

2.2. Preparation of Photocatalyst Composite Membrane Mats. PVAc was solubilized in DCM at 4 and 6% concentrations (wt %) at 28.5 °C (room temperature). Following total polymer dissolution, TiO_2 in two concentrations (namely 5 and 10 wt %, based on the polymer solution,) was added to the optimized polymer solution (6%) to improve the properties of nanoscale fibers. This mixture was vigorously stirred for more than 18 h followed with 1 h sonication at room temperature to produce well-dispersed NPs in the polymer solution. The mixing process is based on solution blending method where the polymer and inorganic phases are connected by van der Waals forces or hydrogen bonds.[21] This solution mixing method is a facile way to prepare polymer-inorganic composite solution and suitable for all kinds of inorganic materials where the concentration of the organic and inorganic components is easy to control. Solutions viscosities were measured by a Brookfield, DV-III ultra programmable Rheometer at room temperature and the results are listed in Table. 1.

Table 1. Viscosity Measurements of PVAc and TiO_2/PVAc Solutions

	4/96 PVAc/DMC	6/94 PVAc/DMC	5% TiO_2 mat	10% TiO_2 mat
viscosity (cP)	35.1	285.4	328.3	430.1
torque %	1.3	11.9	13.1	17.8

Each prepared solution (two pure PVAc solutions and two TiO_2/PVAc suspended solutions) was injected into a custom designed airbrush spraying apparatus (Pa-201, IWATEC, Taiwan; Figure 1A) at room temperature and 40% humidity with a nozzle that had a diameter of 250 μm, double action/internal mixing capability and a gravity fed color cup. We used two different solute concentrations (4 and 6 wt %), while keeping other processing parameters constant, and the duration of spraying was controlled to ensure that the total mass of the polymer blend delivered to each surface remained also constant. At all solute concentrations, AJS nanofibers layer formed in 1.45 min (15 mL/min) was found to rapidly cover the collected substrate (12 × 5 cm^2). The designed AJS system consists of a customized atomizer that plugged into compressed medical grade air (420 kPa) and filled with the as-prepared solutions through a fed color cup based on gravity-controlled rate. The distance between the collector and the AJS tip was 30 cm which was optimized according to our previous publications.[15,17] We observed that the variations in the spraying distances within this distance range can create interconnected and well-defined fibers. The airbrush was automatically fixed using a novel AJS system by our research group, in which the whole AJS setup was enclosed in a sealed chamber and maintained at room temperature (seeFigure S2 in the Supporting Information).The spinning fibers were directly deposited on rotating collector (speed, 60 m/min). To compare between the pristine fiber mats prepared by AJS and those prepared by electrospun process, PVAc fibers were prepared by electrospinning using an apparatus and process described previously.[22,23] Briefly, the electrospinning power supply was connected to the metal capillary tip. The voltage was 21 kV, and the tip-to-collector distance (TCD) was 14.0 cm. The droplet instantly disintegrated into spinning fibers, which were drawn onto a grounded substrate (Figure 1B). After the fabricated mats were dried in a vacuum oven for 24 h at 30 °C the mats were annealed at 6 °C to provide an additional strength.

2.3. Membrane Mat Characterization. Membrane mats layer thickness was assessed by ultrasonic measurement (coating thickness gauge meter OMEGA instrument, OM179−745) with a precision of ±1.0 μm. The membrane mats surface topography was characterized using a scanning electron microscope (SEM, JEOL, JSM 820, Japan). All specimens were freeze-dried and coated with a thin layer of gold before SEM observation. The average fiber diameter, porous mean size, and porous distribution of the prepared mats were calculated for three different specimens using image analysis software (ImageJ, National Institutes of Health, USA, http://imagej.nih.gov/ij/). The porosity of the pristine and composite prepared mats were calculated using the following equations according to a previous study[24,25].

$$\text{density of mat}(\text{g/cm}^3) = \frac{\text{mat mass (g)}}{\text{mat thickness (cm)}\cdot\text{mat area (cm}^2\text{)}} \quad (1)$$

$$\text{porosity (\%)} = 1 - \frac{\text{density of mat (g/cm}^3\text{)}}{\text{density of used materials (g/cm}^3\text{)}} \quad (2)$$

The nitrogen adsorption−desorption isotherms which were measured at 77 K using Monosorb, USA apparatus were used to investigate the Brunauer−Emmett−Teller (BET) specific surface areas of PVAc/TiO_2 composite photocatalyst membrane samples as descripted previously in our study.[22]

The phase composition of fabricated samples surfaces was analyzed by glancing-angle X-ray diffraction (GA-XRD, Philips X'Pert, Holland) using Cu K_α (k = 1.54056 $A°$) radiation over 2 h range angles from 5 to 80°. The operating voltage and current used were 40 kV and 30 mA, respectively, with a beam size of 20 μm. FT-IR spectra in transmission mode were collected using an ABB Bomen MB100 spectrometer (Bomen, Canada) to investigate the phase composition and any phase interaction between the compounds. Thermogravimetric analysis (TGA) was used to determine the loading of TiO_2 NPs within the polymer matrix. The TGA measurements were conducted using SDT Instruments SDT Q600, Elmer Inc., USA, under nitrogen atmosphere over the temperature range of 25−600 °C at a heating rate of 10 °C/min.

2.4. Wettability. The hydrophobic or hydrophilic properties of the as-fabricated membrane mats were measured with deionized water contact angle measurements using a contact angle meter (Digidrop, France). Deionized water drops (6 μm in diameter) were automatically dropped on each AJS mats. AJS fibrous mats (5 × 4 cm^2) of different samples were measured four times for each sample. The contact angles were measured immediately after deionized water was allowed to fall freely onto the surfaces of the flat nonwoven mats and STD was calculated.

2.5. Mechanical Properties of the AJS Composite Nanofibers. The mechanical properties of the fabricated samples were carried out according to our previous studies.[26] The pristine and composite mats were tested using a tabletop tensile tester (Instron LLOYD Instruments, LR5K Plus, UK) with a load cell of 100 N. Testing was performed at a crosshead speed of 10 mm min^{-1}. Four to five specimens were used for each sample and were expressed as the mean ± standard deviation. Stress−strain curves were plotted to

DOI: 10.1021/acsami.5b01418
ACS Appl. Mater. Interfaces 2015, 7, 13329−13341

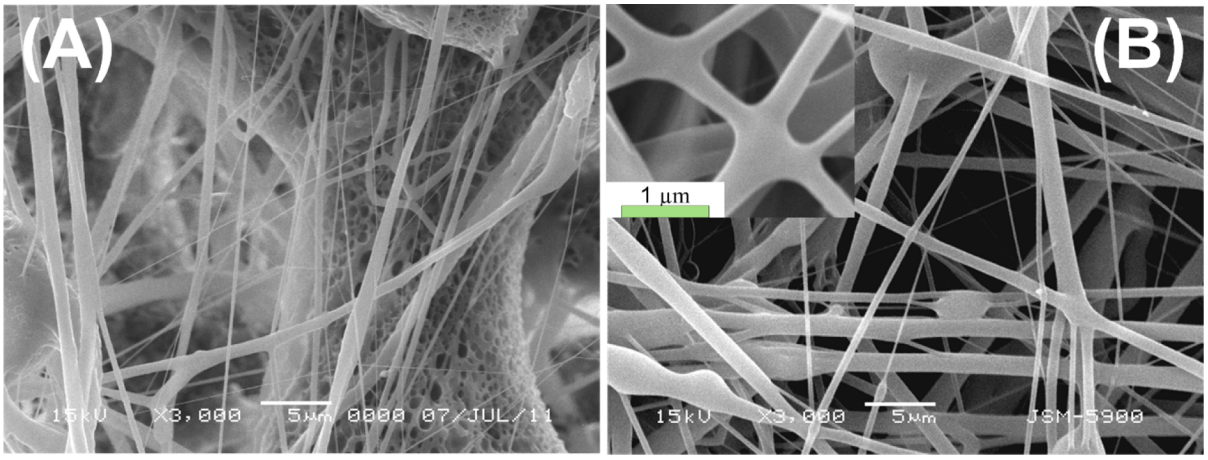

Figure 2. SEM photographs of AJS PVAc pristine membrane sample with two different solution concentrations: (A) 4 wt % and (B) 6 wt % PVAc concentration. Inset of panel B shows interconnected bonding structure fibers.

calculate the tensile properties in terms of the ultimate tensile strength, Young's modulus and breaking elongation of the nanofibers scaffolds. All of the samples were tested after being conditioned in a laboratory environment for 24 h under identical conditions.

2.6. Adhesion Performance. The adhesion (pull off) tests were used to investigate the adhesion strength of the directly deposited layer-by-layer formed by AJS at the same distance between the AJS tip and three different ground substrates. The three ground substrates are watch glass with thickness 4 mm and diameter 12 cm, commercial pure titanium sheet with thickness around 2 mm and diamter 25 mm with the chemical compositions shown in Table S1 of the Supporting Information, and a plastic sheet made from PLLA material with rectangular dimension of 2 cm × 8 cm. The adhesion tests of the coated samples were performed under dry conditions at room temperature. After drying the coated substrates, the dolly secured with adhesive under a static load using Araldite Epoxy adhesive, which was cured at room temperature for 24 h. Subsequently, the pull-off test was conducted using the Elcometer Adhesion tester (England). Three samples were tested for each coating substrate and the reported data represent the mean of these measurements.

2.7. Photocatalytic Activity Measurements. The photocatalytic activity of the as-prepared photocatalysts materials was measured by observing the degradation of methylene blue (MB) dye solution in a simple photochemical reactor, as described elsewhere.Briefly, the reactions were conducted in a crystallizing dish (Duran) of 300 mL capacity by immersing the photocatalyst mats in 200 mL of MB dye solution (concentration: 1.5×10^{-5} M) in Petri dishes under sunlight. The experiment was conducted in a natural atmospheric environment on a sunny day (between 11 AM and 2 PM) in September in Charouk, South Korea, with average amount of solar radiation 16.21 MJ/m^2). Photodegrdation properties were investigated by immersing the pristine and composite mats in MB dye solution and cover them with aluminum foil followed by stirring in dark for 1 h to ensure the complete adsorption of MB dye. The dish containing photocatalysts was exposed to the sunlight. The samples were withdrawn at regular intervals of time, and the concentration of the dye was measured by recording its absorbance at 663 nm wavelength with a UV−visible spectrophotometer (HP 8453 UV−vis spectroscopy system, Germany), from which the degradation efficiency of the photocatalyst was calculated. The 663 nm wavelength is chosen due to it is the main UV−vis absorption peak of MB and can be easily monitored during dye degradation (as illustrated in Figure S2 in the Supporting Information).

The durability of the repeated use of the AJS composite fibrous mat was evaluated. Our results showed that the as-prepared photocatalyst composite mats can be used repeatedly without a significant decrease in its efficiency. Therefore, we are expecting that this material will be a promising purification media for contaminated water and air. In fact, some tests were performed at least three times to confirm a final conclusion. We followed very systematic procedures to achieve and optimize our results by using several evaluation techniques supported by several characterization tools to confirm our findings.

3. RESULTS AND DISCUSSION

3.1. Characterization and Morphology of the Polymer/TiO_2 Nanofiber Composites Membrane. Our previous study showed that changing the solution concentration of the dissolved polymer is one of the most effective schemes to alter the membrane morphology.[15,17] This finding was also verified in the present study. The morphologies and the diameter size distribution histogram of AJS pristine mats are shown in Figures 2 and 3, respectively. SEM images revealed

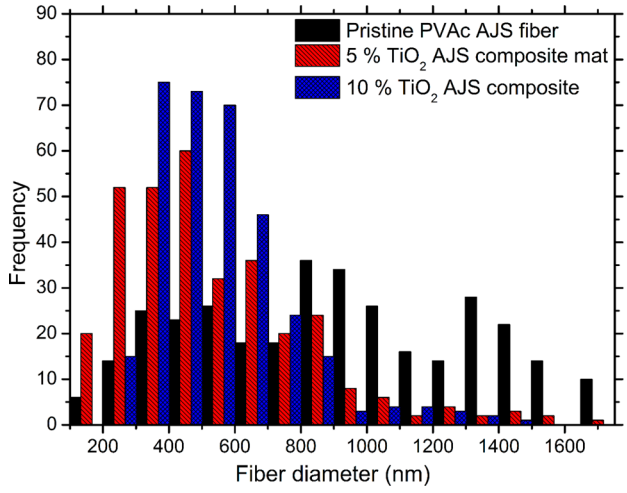

Figure 3. Fiber diameter distribution of AJS membrane fiber mats.

formation of a layer with interconnected porous structures combined with some locally oriented fibers at 4% solute concentration (Figure 2A). As the solute weight ratio increased to 6%, an interconnected bonded (point-bonded fibrous, inset of panel B), smooth, and beadless nanoscaled fiber mat was formed (Figure 2B). Our results confirm the possibility for obtaining fibers with diameter 901.5 ± 32.8 nm, (Figure 3) using AJS. SEM images (Figure 2B) also highlights that the PVAc nanofibers have extremely small diameters.

3.2. Mechanism of Formation of Polymer/TiO_2 Nanofiber Composite Membrane. The cause and mechanism of

DOI: 10.1021/acsami.5b01418
ACS Appl. Mater. Interfaces 2015, 7, 13329−13341

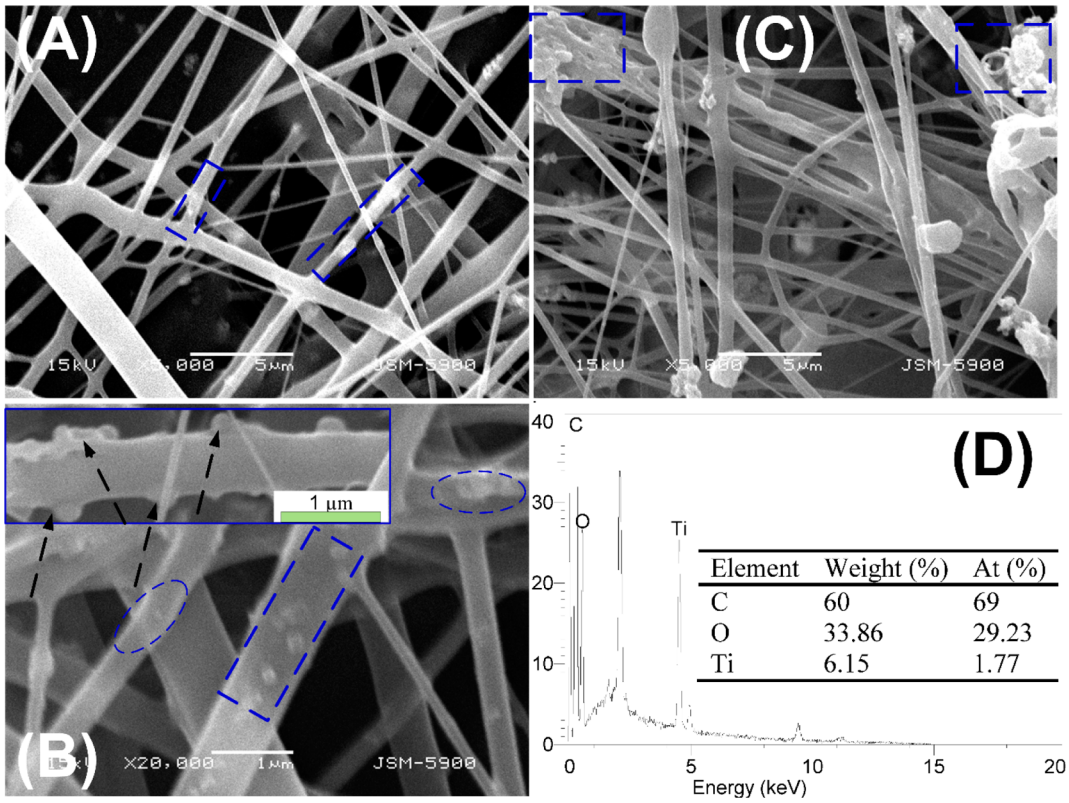

Figure 4. SEM photographs of (A, B) 5 wt % TiO_2 and (C) 5 wt % TiO_2 AJS composite fiber mats, and (D) SEM-EDS and element concentration of the composite fiber mat. Inset of panel B shows embedded TiO_2 NPs on individual surfaces of AJS PVAc fibers. The selected areas demonstrate the loading of TiO_2 NPs.

the formation of interconnected porous bead and bonded nanofiber structures by means of AJS were explained in our previous work.[17,26] High-magnification images shown in the inset of Figure 2B enabled us to visualize how the PVAc nanofibers were interconnected. PVAc fibers seem to be linked by "'fusion-like'" junctions (inset of Figure 2B). Whether these junctions are associated with remaining solvent or mechanical bonding remains unclear. Regardless of their origin, these junctions led to a better cohesion of the PVAc nanofiber mesh. The presence of interconnected fibers as seen in SEM image in Figure 2, we believe, will be extremely beneficial for water treatment applications owing to their greater filtration accessibility. Barhate et al.[27] illustrated that improving the interpore connectivity in the web enhances the filtration capability of the web and the interfiber bonding makes the web rigid and mechanically stronger (by improving the tensile strength). The diameter size distribution of fibers produced by AJS of polymer solutions containing PVAc were also comparable to fiber diameters of electrospun fibers reported elsewhere.[23,28] When examining the PVAc AJS mat nanofibers using SEM, a similar nanofiber diameter and morphology was observed in different locations in the mat, indicating that air spun nanofiber mats were uniform (data are not shown here).

The deposition of TiO_2 NPs on PVAc fibers using the simple AJS technique discussed in this article will provide new insights toward the fabrication of a durable high-performance photocatalyst. The optimized membrane fibers created at higher dilute solutions were used in a subsequent study by adding TiO_2 NPs to the PVAc solution in order to produce a nanocomposite suspension for photocatalytic application. The nanocomposite suspension was subsequently spun under the same conditions used previously to obtain TiO_2/PVAc composite membrane mats. Our results confirmed that the incorporation of TiO_2 NPs into the polymer solution does not have any negative effect on AJS nanofiber formation performance. It was expected that when a large amount of TiO_2 powder used, jamming problems with the air-spinning system can occur. Surprisingly, the results showed that further loading of TiO_2 NPs into the PVAc solution decreased the fiber diameter size. To prove our results, we measured the diameter size distribution using imageJ software analysis from at least three SEM images for each composite membrane mat. The results of histogram distribution and selected SEM images are shown in Figures 3 and 4. Interestingly, 5% TiO_2 mats showed uniform nanofiber through their longitudinal direction with free-beads formation and interconnected fibers with fiber diameter of 526.7 ± 26.2 nm. With further NPs loading (10%), average diameter size of composite nanofibers was further decreased to 505.8 ± 41.6 nm (Figures 3 and 4). This was attributed to the fact that the loaded TiO_2 particles did not hamper the uniform jet initiation and further elongation into fibers. The possible reasons for decreasing fibers diameter size with further TiO_2 NPs loading may be due to increasing the composite solution viscosity after the incorporation of NPs, as shown in Table 1.

The viscosity of the polymer is among the critical factors that can affect the morphology of spinning fibers.[29] In this article, the viscosity of TiO_2/PVAc solution was changed remarkably by adding TiO_2 (Table 1), indicating a change the morphology of AJS fibers. Accordingly, we argue that high TiO_2 NPs concentration and solution viscosity might have played a significant role in production of lower nanometer range fibers. This can be explained by the fact that the TiO_2/PVAc spinning

DOI: 10.1021/acsami.5b01418
ACS Appl. Mater. Interfaces 2015, 7, 13329−13341

Table 2. Some Membrane Structural Parameters of the Fabricated Samples

sample	diameter size (nm)	thickness (μm)	average pore size (μm)	BET (m^2/g)	porosity ($\sim$ %)
elecrospun pristine PVAc fiber	325.4 ± 61.9	77.22 ± 11.1	1.38	27.22	72
AJS pristine PVAc fiber	901.5 ± 32.8	85.12 ± 6.5	4.23	7.15	91
5 wt % TiO_2 mat	526.7 ± 26.2	87.22 ± 9.41	5.12	328.70	93
10 wt % TiO_2 mat	505.8 ± 41.6	89.00 ± 14.3	1.58	72.13	79

solution became more viscous with increasing the amount of TiO_2. Consequently, this could decrease the solution flow rate (feed rate) flowing from the gravity feed cup of AJS, resulting in a lower feed rate and much thinner fibers, as shown in Figure 4A, B. Further reasonable reason is likely that the AJS basically uses the energy stored in high pressure compressed air to propel a solution at high velocities to the output of throat. On the basis of these hypotheses, we proposed a possible mechanism for the formation of composite nanofibers mat structure, as shown in Figure 1A. At the throat section shown in inset of Figure 4A (noted as b), the deposited particles slightly reduced the diameter size of the throat, resulting in reduction of the ejected solution to lower amount through the throat of AJS. Subsequently, the solution amount of stretched fibers can be controlled. The same observation was reported by Francois et al.[30] where they noticed that a high polymer flow rate can stimulate the formation of polymer droplets that smashed the fibrous mat. This undesirable effect was alleviated by maintaining the polymer at the lower selected flow rate values. The change in fiber diameter can provide an opportunity to fine-tune the membrane porosity.[31] Successful AJS of the TiO_2 NPs-loaded PVAc nanocomposites provided further evidence of the excellent spinnability of AJS with respect to previous PVAc spinning formulation. In contrary, the increase in fibers diameter with viscosity has been reported for many electrospun polymer fibers.[13,32] The presence of inorganic NPs in the electrospun solution increases the diameter of the polymeric nanofibers during electrospinning.[13,32] A higher NPs contents adversely affected the electrospinnability of the polymeric solution (blocking the tip of the syringe at higher concentration was also observed[33]). Hence, there are significant differences between the fibers spinning using AJS and electrospinning techniques. The AJS is based on ejecting (blow spinning) the polymer solution to output nozzle using pressurized gas, whereas electrospinning is based on stretching (pull out) of the polymer solution under high potential static voltage. This means that the larger amount of suspension could not facilitate the electrospinning process for the formation of smaller diameter fibers.

TiO_2 nanoparticles can be agglomerated in organic solvent−polymer solution due to the residual surface OH groups exists on NPs. Because of the fluctuation of NPs inside AJS jet and the plastic deformation between the NPs and fiber substrates during AJS, the NPs could be easily dispersed and completely combined with PVAc fiber surface. Our results showed that AJS TiO_2/PVAc composite nanofibers mat formed at 5 wt % TiO_2 NPs are well-embedded uniformly onto and around the polymer fiber surfaces (Figure 4A, B). Conversely, the TiO_2 NPs were agglomerated on the fiber surfaces and inside the matrix in case of 10 wt % TiO_2 (Figure 4C). At lower TiO_2 loading (5 wt % TiO_2), NPs were well-dispersed and stick onto the top surfaces of individual fiber as clearly shown by the marked dashed box and higher magnified image in Figure 4B. On the other hand, larger particles sat between interfiber spaces and some amount of aggregation were occurred, imparting a rough texture to the substrates during the higher particles loading (10 wt % TiO_2) as shown in Figure 4C. In this case, the nanocomposite fiber surfaces were found to be irregular and uneven exhibiting protruded granulate-like morphology, presumably because of the aggregation of TiO_2 NPs. TiO_2/polymer composite were prepared by Pant and his co-workers[32,34] fabricated electospinning composite nanofibers mats at the same concentrations (5 and 10% TiO_2). They showed that TiO_2 NPs were agglomerated and heavily loaded mass on some parts of composite fiber matrix. This reveals that our preliminary results of immobilization TiO_2 particles on nanofiber surfaces using AJS could show better morphological structure properties than that previously prepared.

3.3. Effect of Spray Particle Velocity on the Spinning Fiber Morphology. In general, as mentioned above, an air spray accelerates the polymer ejection through a needle, stretching it to form nanostructured fibers (Figure 1A). Hence, the basic principle of the jet-spinning process is very simple. A high velocity air jet, further formed using a converging-diverging nozzle (inset of Figure 1A, noted as a), is used to accelerate TiO_2/PVAc composite solution and spin them onto a substrate. Accordingly, the most important parameter of spray particle in AJS process is its velocity prior to impact on surface substrate. The particles that are suspended in a polymer solution fluctuate through a convergent−divergent nozzle (Figure 1A) of AJS and upon impact with the prior spinning fiber substrate; the particles were well-embedded and adhered onto the fiber surfaces. The kinetic energy of the particles, supplied by the expansion of the gas, is converted to plastic deformation energy during bonding. This allows intimate conformal contact between the exposed polymer fiber surfaces under local pressure, permitting bonding to occur between the components. It is accepted that the kinetic energy of the particles is higher than that of the polymer molecules (because of a higher mass). This helps the particles to plastically deform on impact and form strong interfacial bonding with spun fibers, which bond together to produce advanced composite mat. This can avoid or minimize many deleterious shortcomings of traditional method such as electrospinning process. In this process, TiO_2 particles were fluctuated inside the convergent-divergent airbrush nozzle and subsequently accelerated by the high-speed gas jet at a room temperature, resulting in precipitating of TiO_2 NPs onto each single spun fibers. The surface distribution of the photocatalyst membrane composite mat formed at 5% TiO_2 is more uniform than that formed 10% TiO_2. Our previous work showed that PVAc could be air spun,[17] whereas the current work demonstrates that nanofiber membrane composite mats composed of PVAc and TiO_2 NPs could be air spun too.

3.4. Filtration Efficiency of Polymer/TiO_2 Nanofiber Composites Membrane. The filtration efficiency is normally influenced by the filter physical structure, such as membrane thickness, matrix structure, pore size, porosity, etc.[27,28] Table 2 shows that the thickness of the membrane mats based on 6 wt % PVAc solution after a short time, 1.45 min, of air spinning

DOI: 10.1021/acsami.5b01418
ACS Appl. Mater. Interfaces 2015, 7, 13329−13341

deposition was on the order of micrometers. Pore size and porosity are important parameters in membrane structural that influence the performance of water filtration and dust holding capacity of the filter, thus porosity should be adequate enough to avoid the pressure drop.[28] Conventional ultrafiltration or nanofiltration filters for water treatments are based on porous membranes.[31] Porous polymeric ultrafiltration membrane fabricated by the phase immersion method (conventional method) has its harsh limitations, e.g. low flux and high fouling tendency due to geometric structure of pores and the corresponding pore size distribution and undesirable macrovoid formation across the whole membrane thickness.[35] Our results showed that the nonwoven membranes prepared by the AJS method could be highly porous with excellent pore interconnectivity (Figures 2 and 4) than that of nonwoven membranes prepared by conventional electrospinning process (Figure S4 in the Supporting Information). Nanofibrous membrane mat should have a much higher flux than conventional nonporous membranes in ultrafiltration or nanofiltration filters.[35] The AJS membrane mat exhibited the highest porosity value, which was significantly higher than the values determined from commercial ultrafiltration (e.g., Pall Corporation) and nanofiltration (e.g., Amicon XM300) filters and more than 2.5 times larger than that of Millipore HAWP microfiltration filter (~34%). The average pore size (i.e., flow-through pore size) of pure PVAc nanofibers membrane prepared by AJS and electrospinning process were 4.23 and 1.38 μm, respectively. AJS nanofiber membrane showed porosity of about 91%, which is higher than conventional electrospun PVAc nanofibers that showed 72% porosity. To further verify our results, the specific surface area (BET) of the as-prepared membrane mats were measured in this study. The BET of pristine mat obtained using AJS fibers was about 3.8 times lower than that of electrospun mat fibers (Table 2). The difference in porosity and BET measurements can be noticed by SEM examination which showed that AJS nanofiber mats were loosely packed with large voids (few fiber mass per unit area) (Figures 2 and 4), whereas electrospun nanofibers were more tightly packed and entangled (Figure S4 in the Supporting Information). AJS nanofiber membrane mats had bundles of aligned nanofibers in some local areas, which crossed one another to create larger pores, lower BET and subsequently higher porosity. Conversely, electrospinning nanofibers mats had single nanofibers that were more tightly packed with smaller pore size and lower porosity. Our results are in a good agreement with the previous reports data by Tutak et al.[36] The torturous porosity in electrospun membranes usually results in a relatively low flux rate.[31,27] AJS demonstrated a new type of high flux ultrafiltration/nanofiltration medium based on a nanofibrous membrane mat. The benefit of adjustable pore size and high porosity is extremely attractive for the study in water treatment applications. It was reported that the well-interconnected adequate pores in the nanofiber mat warrant effective interactions between the reactant and catalyst, which is valuable for continuous-flow chemical reactions or biological processes.[28]

The porosity of the as-prepared AJS composite membrane mat increases and then decreases slightly with the increase of the TiO_2 content. The BET specific surface area of the TiO_2/PVAc AJS composite membrane mats illustrated a remarkable difference compared with the pristine mat (Table. 2). The surface area of 5 and 10% TiO_2 mats were around 328.7 g/m^2 and 72.13, respectively. This large difference between the surface fiber mat before and after TiO_2 loading might be increased due to the presence of TiO_2 NPs on/within the fiber matrix. The measured porosities are 93 and 79% for 5 and 10% TiO_2 membrane mats, respectively. The average pore size of the membrane with 5 wt % TiO_2 content increased and then decreased with increasing TiO_2 content to 10% because of the particle aggregation, and there are not enough free surfaces to equilaterally distribute the particles onto the fiber mats, which also might be the same reasons for decreasing the surface area of 10% TiO_2. However, the average pore size between nanofibers demonstrated that these mats have still micropores with a narrow distribution (Figure 4B, C): The mean pore size of 5 and 10% TiO_2 mats was 5.12 and 1.58 μm respectively (Table 2). As demonstrated 5% TiO_2 mat showed higher porosity than both pure PVAc and 10% TiO_2 mats. The variations in the fiber diameter could partially change the interconnected porosity of the nonwoven nanofibrous mat under our experimental conditions. It can be concluded that with proper control of the processing parameters, fibrous membranes with significant porosities and pore size can be made using AJS strategy. These characteristics are due to (a) high porosity, (b) interconnected open pore structure, and (c) tailorable membrane thickness.[27] On the basis of these results, we expect that the developed AJS nanofibrous membrane mats can replace the conventional porous membranes and exhibit a much higher flux rate for water filtration.

3.5. Thermogravimetric Analysis. One of the challenges with the polymeric membrane is their low thermal stability to cope with the harsh process conditions of temperature and pressure.[37] Loading of TiO_2 particles and their effect on the thermal stability of the AJS composite membrane mats were evaluated via thermogravimetric analysis (TGA), whereas thermal stability plays an essential role in determining both technological applications and processing conditions of polymeric nanocomposites. SEM-EDX analysis was performed to affirm that the TiO_2 was present in the composite mat. Figure 4D confirmed that TiO_2 particles were loaded on the polymeric nanofibers. Figure 5 shows the TGA data as weight loss vs temperature. A systematic change is clearly shown in the decomposition temperature, weight loss and residue left as we incorporate more TiO_2 particles to the PVAc matrix. Pure PVAc mat starts to decompose around 300 °C and continue

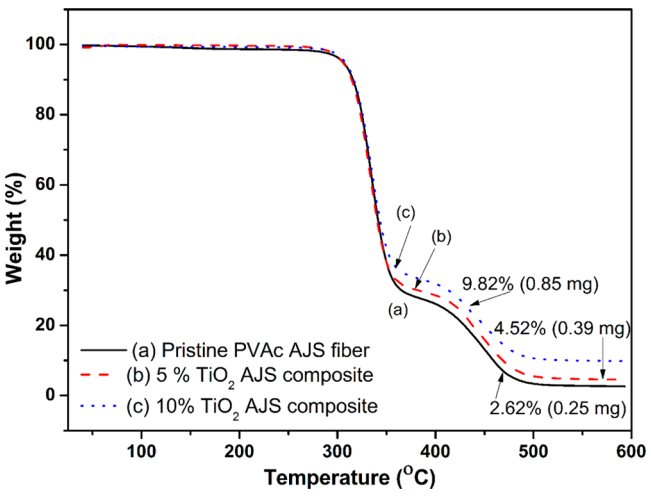

Figure 5. TGA curves of AJS pristine PVAc mat and different amount of TiO_2 containing nanocomposite mats.

DOI: 10.1021/acsami.5b01418
ACS Appl. Mater. Interfaces 2015, 7, 13329−13341

decomposing until around 500 °C which is consistent with the previous reports.[38] In a good agreement with our results, previous study on the thermal degradation performance of polyvinyl acetate reported that degradation takes place in two steps such that around 72% in the first step and around 25% in the second step.[39] Pure PVAc polymer leaves some residue after two stages of mass loss (2.62%) and that was attributed to the char formation because of high temperature.[40] When we incorporate TiO_2 particles to PVAc matrix, the decomposition curve was shifted to the right and upside. With increasing the amount of particles in the AJS CPM mat, the wt % of the residue increases indicating the presence of TiO_2 particles within the AJS composite mats at different amount. Considering the polymer degradation, it can be urged that the wt % of the residue left has increased with further addition of TiO_2 particles. This increase in the residue content is important to be considered when explaining the thermal stability of the AJS TiO_2/PVAc CPMs. The onset degradation temperature of the nanocomposites was slightly increased with TiO_2 content. This improvement in the thermal stability can be attributed to the presence of nanofiller (Figure 4A–C). It is likely that the TiO_2 NPs increase the surface sites for the chemisorption of PVAc that would not be available when pure PVAc is decomposed. It seems that both PVAc and TiO_2 have been integrated on molecular level and a new composite material has been formed using AJS with improved thermal stability.

3.6. X-ray Diffraction and FTIR Analysis. The XRD patterns of as-received nanosized TiO_2 crystal powders and as-prepared membrane mats are shown in Figure 6a–d. The

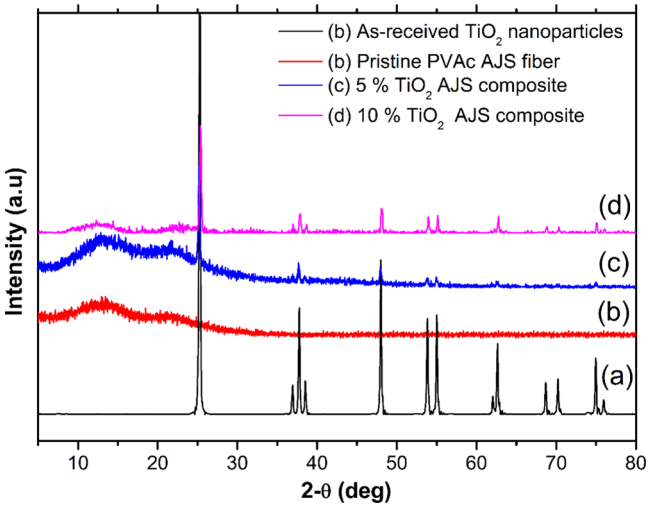

Figure 6. XRD patterns of as-received TiO_2 NPs, pristine, and composite AJS membrane fiber mats.

pattern of TiO_2 crystal powders showed different crystalline characteristic peaks as shown in Figure 6a, which quantitatively agrees with the crystallographic compositions of the as received powder as well as the reported literature.[22] The pattern of the TiO_2/PVAc composite mat also showed same crystalline characteristic peaks analogous with the characteristic peaks of TiO_2 crystal powders.[22] The characteristic peak intensity of PVAc (2θ = 13°) increased at 5% TiO_2 loading onto CPM matrix (Figure 6c) in comparison with pure PVAc intensity peak (Figure 6b). This can be related to the occurrence of some hydrogen interaction bonding between the particles and the polymer chain molecules during AJS spinning. In other words, a plastic deformation can occur upon impact of TiO_2 particles onto AJS spun fibers causing a polymer chain mobility and thereby induced chain conformation on PVAc molecules. The intensity of the TiO_2 peak increases as the content of TiO_2 increases in the AJS CPM mats and both PVAc and TiO_2 peak positions are lightly shifted toward the right compared to the peaks for the pure form, further supporting the likely occurrence of an interaction bonding. The intensity of PVAc peaks reduced with increasing theTiO_2 content (Figure 6d). The primary crystalline pattern in the PVAc due to hydrogen bonding between hydrogen of alkyl groups is being disrupted by the further addition of TiO_2. This can be explained by the particles aggregation of high TiO_2 loading resulting in a decrease in the PVAc crystallinity compared to the lower TiO_2 loading.

To confirm the observed changes from X-ray profile, we performed vibrational spectroscopy, which is more sensitive to the molecular conformation of polymers.[41] Vibrational spectroscopy showed similar trends to those of the X-ray profiles. The IR spectra of different mats (Figure 7) showed a significant

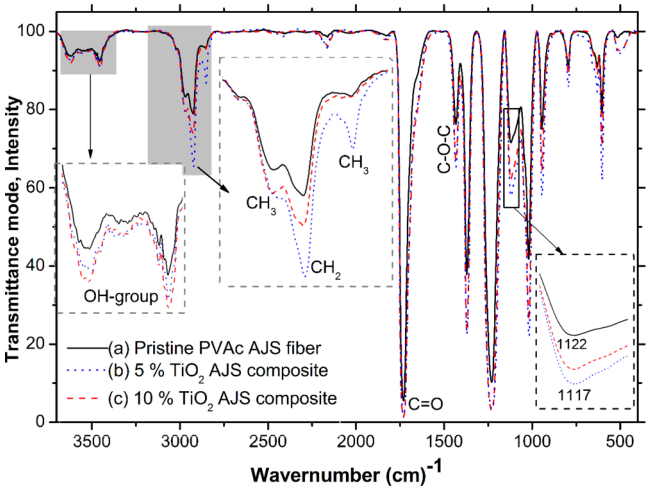

Figure 7. FTIR profiles of pristine and composite AJS membrane fiber mats.

effect on the crystalline structure of AJS PVAc mats due to the TiO_2 addition. Interestingly, the IR bands of the as-prepared nanocomposites become sharper and stronger than that of the pristine polymer fibers after loading TiO_2 NPs to the fiber matrix. This indicates the strengthening of hydrogen bond in the composite mat. Further increase in the intensity of these bands in 5% TiO_2 mat revealed that hydrogen bonding increased due to the well-dispersed TiO_2 onto the fiber surfaces (Figure 4B). We noticed that the several peaks of PVAc (inset of Figure 7) become sharper, which further proves some interaction between TiO_2 and PVAc. Our previous work[26] showed similar performance that the AJS process significantly improved the interaction by embedding nanoparticles onto the fibrous surface during air spun process. The possible mechanism of PVAc and TiO_2 combination in the CPNM matrix may be one as briefly mentioned in the Introduction section, where Ti–OH groups on the surface of TiO_2 can react with the alkyl group hydrogen of the PVAc chain, making hydrogen bonding at the interface. Hence, well-dispersed TiO_2 NPs at high impact force could rupture the intermolecular hydrogen bonds of PVAc chain and form new hydrogen bonds

DOI: 10.1021/acsami.5b01418
ACS Appl. Mater. Interfaces 2015, 7, 13329–13341

between TiO_2 and PVAc molecules. This observation confirms the results of XRD where the addition of TiO_2 NPs to the PVAc using AJS has modified PVAc crystallinity, which is consistent with the reported literature showing similar effect.[26] The permeation results (Figure 7) showing an increase in the hydrogen bonding upon the addition of TiO_2 to PVAc also suggest the creation of strong chemical interfacial bonding between the NPs and polymer molecules using AJS process. Previous reports by Ahmad and Hagg[37,42] using PVAc/inorganic NPs mixed matrix membranes did not induce chain conformation on PVAc molecules and showed poor interfacial bonding between the components. This further proves that our developed AJS process has a strong affinity to strengthen the hydrogen bonding of pure and composite matrix. Therefore, we expect that the successful deposition of TiO_2 NPs on the surface of PVAc fibers with a strong interfacial bond will make this composite as an effective photocatalyst in terms of the enhanced photocatalytic activity and the stability of the photocatalytic particles. The newly developed AJS membrane mats are expected to strengthen the interface significantly through the maximizing of hydrogen bonds with a positive impact on the mechanical properties.[27]

3.7. Mechanical Properties of Polymer/TiO_2 Nanofiber Composites Membrane. However, the AJS process produces "nonewoven" randomly orientated mats which result in extreme difficult of the accurate measurement of the stress–strain curves, we concern on the effects of TiO_2 NPs loadings to the polymer matrix on mechanical integrity of composite membrane mats as a preliminary study. The representative stress–strain curves of the AJS fibrous membrane mats are shown in Figure 8 and Table 3. Interestingly, the AJS fibrous membrane mats yielded drastically different tensile performance despite sharing the same specimen size, dimensions, and loading rate (10 mm/min). The tensile strength of the pristine mat was about 14.72 MPa, whereas that of the composite scaffolds was greater than that of the neat one, with the property value ranging between 22.3 and 32.13 MPa (see Table. 3). The peak value of tensile strength should not be reached at a TiO_2 concentration as low as 5 wt % (Table. 3). Poor dispersion and weak interfacial contact of the TiO_2 at higher concentration (10 wt %) of NPs may be responsible for the observation that maximum tensile strength occurred at a lower concentration. The steeper slope of the curves proves that the Young's modules of the composite nanofibers are significantly increased. The trend of stress–strain curves shows a higher value in Young's modulus (121.65 MPa) at 5 wt % TiO_2. The strain to break became smaller with increasing the TiO_2 concentration.[22] This significant stiffening can be attributed to the high stiffness and high aspect ratio of the incorporating NPs and is comparable to results reported from HA-reinforced PLA fibers.[26]

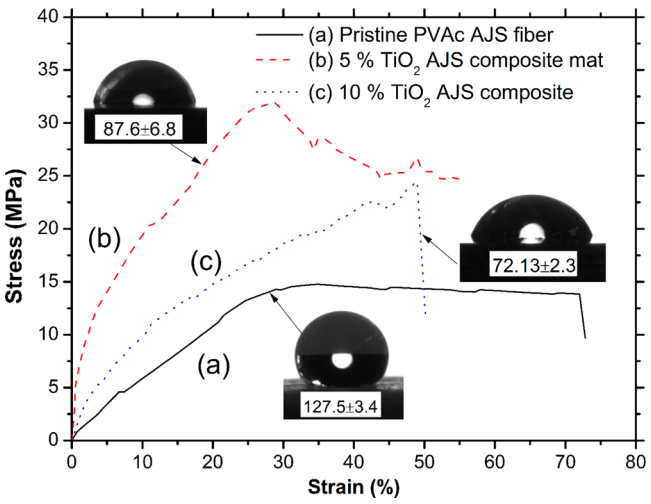

Figure 8. selected typical stress–strain curves of AJS pristine and composite membrane mats. Insets are their water contact angle correspondingly.

The TiO_2 NPs provide an efficient means of stress transfer and reinforcement in nanofibers composites.[43] Hence, the enhanced tensile properties upon incorporation TiO_2 is due to the maximizing of hydrogen bonds and good interfacial bonding between the NPs and the polymeric molecules during AJS process. We can also urge that some NPs were capsulated inside the stretched fibers during AJS process, which restricts the movement of polymer chains. Hence, AJS fabrics are expected to take advantage of the mechanical inter locking mechanism of load transfer between the NPs and nanofibers and thereby creating a local region of enhanced strength, and may significantly enhance the performance of a composite. To confirm our hypothesis, we conducted morphological observation using SEM involving very small amounts (being applied at very short durations of around 2 s) of AJS composite fibers (Figure 9). As expected, we found that the NPs well-capsulated inside the as-spun single fibers (see the inset and selected area in Figure 9). Formation of a strong mechanical inter locking can result in marked improvement in the tensile strength and stiffness of the AJS composite mats. According to previous reports for photocatalyst composite materials prepared using various strategies,[44−49] particularly those focusing on electrospinning,[13,32,50] the load transfer from a matrix to a filler was realized through a weak micromechanical interlocking and chemical bonding between the filler and matrix. One further possible reasonable explanation of the enhanced mechanical properties of the composite mats is that the diameter size of the as-spun nanofibers in the composite mat is smaller than that of pure fiber and that may be responsible for the much higher tensile properties. Wong et al.[51] showed that the decreasing of fiber diameter plays a dominant role in the abrupt increase of mechanical properties (the modulus and strength) of fibers. Indeed, our results strongly indicate that incorporating TiO_2

Table 3. Measurement Values of Tensile and Adhesion Tests

sample	tensile strength (MPa)	Young's modulus (MPa)	breaking elongation (%)	adhesion strength (MPa)		
				glass	metal	plastic
AJS pristine PVAc fiber	14.72 ± 0.85	48.8 ± 7.21	72.2 ± 9	17.14 ± 1.16	9.2 ± 0.7	4.5 ± 0.8
5 we.% TiO_2 mat	32.13 ± 2.1	121.65 ± 12.4	54.1 ± 7.3	7.25 ± 1.14	15.22 ± 0.93	2.3 ± 0.5
10 we.% TiO_2 mat	22.3 ± 1.85	88.65 ± 8.11	49.4 ± 5.8	5.15 ± 2.1	6.23 ± 1.5	1.87 ± 0.45

DOI: 10.1021/acsami.5b01418
ACS Appl. Mater. Interfaces 2015, 7, 13329–13341

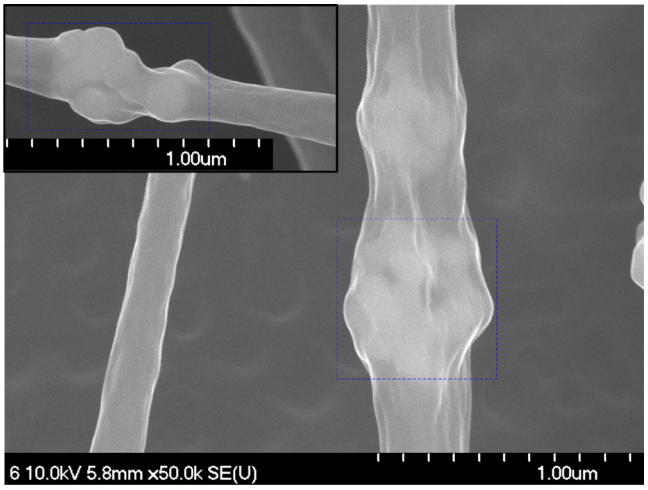

Figure 9. Capsulation of TiO_2 NPs within PVAc fibers using AJS. Inset and selected rectangular areas further illustrate these capsulated NPs.

nanofillers using AJS can be a promising approach to be utilized for fabrication of high strength nanofibers.

3.8. Adhesion Performance of AJS Membrane Fibers on Different Substrates. As the sustainability of drinking water availability is challenged worldwide, nanofiltration is becoming one of the most important technologies in this century for water treatment because of its superb efficiency in producing high-quality water at relatively low costs. We expect that the commercial water/air filters media may be possible tunable by spraying a fiber coating directly onto their surfaces to incorporate additional functionality to the ultrafiltration media such as particle filtration, capture and antimicrobial functionality or catalysts.[27] Recent research work by Podgorski et al.[52] and Lee et al.[3] showed that fibrous filters containing nanofibers are very promising and economic tools to enhance filtration efficiency. Although electrospun membrane scaffolds can be considered as effective filters for liquid filtration, there is a major adhesion problems at the polymer and substrate interface which causes the coatings to peel off easily,[53] which is not the case with AJS technique. The adhesion performance of substrate-coated samples with AJS fibers layer was evaluated using the pull-off adhesion test. Our experiments showed that AJS could be used to deposit nanofibers directly onto different objects made from a wide range of materials (Supporting Information, Figure S5). In the present study, three substrate materials were tested for comparison purposes: (1) a commercial titanium plates treated with alkali solution to increase the hydrophilicity using the same procedures described elsewhere;[54,55] (2) a glass substrate where it possess an advantage as a catalyst support because of its transparency to UV light in photocatalytic applications; and (3) plastic substrate. No differences were observed between the fibers sprayed on glass, metals, and PLA plastic film (data not shown). Typical values for adhesion strength of AJS membrane mats deposited onto these materials substrate are summarized in Table 3. Prior to pull off test, through visual inspection, we found that membrane mat layer was very adherent to both metallic and glass substrates, and it was very hard to peel off by hand. According to the measured pull off data (Table 3), the adhesion of glass substrate coated with pristine PVAc mat showed the highest adhesion, with an average value around 17.14 MPa, whereas the metal substrate coated with 5% TiO_2 mat showed good adhesion, with an average value 15.22 MPa. Samples coated on plastic substrate showed less adhesion performance (Table 3). The reason behind these remarkable differences between the adhesion values is unclear, particularly for glass and plastic substrates. The adhesion performance on metal substrate has been discussed previously.[17,55] The ejected spinning fibers impact the substrate with enough kinetic energy to induce mechanical bonding. During the impact, the NPs and nanofibers entrap into the porous surface structure of Ti substrate and intimate conformal contact combined with high contact pressure. There is an evidence for the deep-impact penetration and locking of the coated materials into these porous structure (The porous surface can significantly improve adhesion integration), as shown in Figure S6 in the Supporting Information. This SEM image shows the material adjacent to the interface, supporting the reason for good adhesion strength of 5% TiO_2 composite mat on treated-Ti substrate with alkali solution. It is accepted that adhesive attraction forces and electrostatic effects at an interface depend on the electrical double layer formed at the junction of two materials. An electrical double layer is produced at any boundary, and the consequent columbic attraction might account for adhesion and resistance to separation.[53] We hypothesize that these mechanical interface and chemical interaction are strong enough to avoid the membrane mat to peel-off from the metal substrate, supporting the theory of metal−polymer matrix interaction. Accordingly, AJS membrane mat layer has provided an excellent adhesion on substrates. However, the exact bonding mechanism in AJS process needs further investigation. A work is currently in progress in our laboratory in order to provide better understanding about the adhesion mechanism on these substrates.

3.9. Photocatalytic Oxidation Efficiency. Pant et al.[34] compared the relative photocatalytic oxidations efficiency of TiO_2 NPs incorporated into the electrospun polymer fibers and pure TiO_2 powder. Approximately the same amount of TiO_2 that was present in mat was weighed and made into a suspension with 25 mL of water. Their results showed that the photocatalytic efficiency of pure TiO_2 NPs and TiO_2 NPs loaded in a polymer matrix mat is almost the same, which confirms that the surface area of the TiO_2 NPs does not dramatically decrease upon the incorporation of the NPs into the polymer fiber. Further, 5 and 10% TiO_2 in electrospun mat showed a negative effect on photodegradation activity; hence, these electrospun mats will not be used in the present study for comparison. The photocatalytic performance of the TiO_2/PVAc composite membrane mats was evaluated by degrading the methylene blue (MB) under natural solar-light irradiation. It was reported that MB may decompose itself under a UV/solar-light irradiation.[49] Lee et al.[3] found that polymeric nanofibers coated with TiO_2 NPs can be used for photocatalytic of organic materials under UV light source. In this work, the plots showing the concentration of MB dye degradation with respect to time is presented in Figure 10. Photocatalytic efficiency of 5 and 10 wt % TiO_2 mats has almost the same performance up to 100 min. After that, the efficiency of 10 wt % TiO_2 is significantly higher than that of composite mat contained 5 wt % TiO_2. It is probably that after the 100 min exposure time, the agglomerated and embedded TiO_2 NPs within the AJS matrix were well-dispersed into MB solution and thereby causes a further increasing the exposed surface area of the photocatalyst materials. The higher the loading of TiO_2, the higher the resulting catalytic activity.[3] Comparing with literature results measured at much higher loadings of TiO_2,

DOI: 10.1021/acsami.5b01418
ACS Appl. Mater. Interfaces 2015, 7, 13329−13341

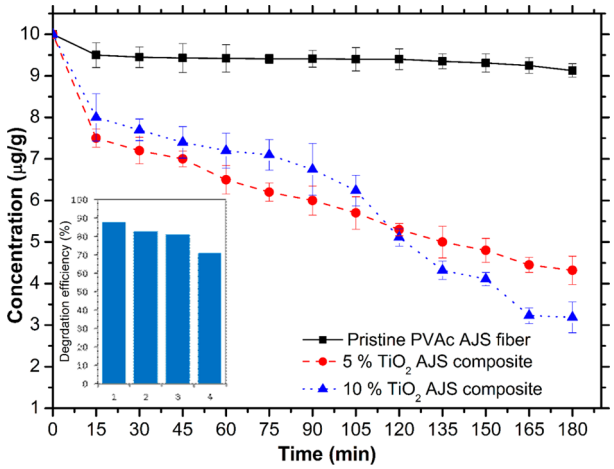

Figure 10. Photocatalytic degradation rate of MB over the different samples under sun light (inset: recyclability of TiO_2 /PVAc nanocomposite mat).

it appears that these membranes show a higher level of catalytic activity. In addition, it could be speculated that the 10 wt % TiO_2 mat has much more hydrophilic properties than 5% TiO_2 mats. The incorporation of highly hydrophilic domains such as TiO_2 into a hydrophobic polymer surface (PVAc is hydrophobic due to its acetic groups) can alter the surface properties of that polymer.[22,56] The photocatalytic activity as well as water filtration efficiency of nanofibers membrane are highly affected by hydrophilicity of the membrane surface.[49] The water contact angles (WCAs) of the prepared photocatalyst mats and the contact angle values of different mats at 1s are given in the inset of Figure 10. The result shows that the 10 wt % TiO_2 mat is not only has a lower WCA than the pure PVAc mat but also slightly more wettability than 5 wt % TiO_2 AJS mats. This difference in water contact angle clearly shows the higher hydrophilicity of 10 wt % TiO_2 mat. It could be due to the presence of TiO_2 NPs on the AJS fibers[22] and may be due to the formation of a greater surface to volume ratio of the 5 wt % TiO_2 composite fibers.[32] The more NPs loading contributes to an additional scale of roughness, which may also serve to lower contact angle.[27] Furthermore, the high photocatalytic activity of 10% TiO_2 composite compared to 5% TiO_2 composite could be due to the high aspect ratio (smaller fiber diameter) of 10% TiO_2 AJS composite mat (Table. 2). Therefore, TiO_2/PVAc composite mats should be highly effective for water treatment.

The durability of photocatalyst is a key issue for practical application. The durability of our samples under the same experimental condition was tested (inset of Figure 10). After four cycles of MB degradation, the nanocomposites still showed comparatively good photocatalytic activity, which proved to be a potent reusable catalyst. Accordingly, it can be concluded that the developed AJS composite membrane mats enhances the efficiency of MB dye degradation under visible light.

Lee and his group[3] stated that fabrication of polymeric nanofibers coated with photocatalytic materials and processing high photocatalytic activity without the deterioration (such as, degradation) of polymeric substrate remains a big challenge. To investigate this hypothesize using FTIR analysis, we have examined the phase structure changes of polymeric substrate decorated with and without TiO_2 NPs after exposure for MB dye degradation under UV solar light at environmental temperature for 2 h (Supporting Information, Figure S7A, B). The IR results of UV irradiation were compared with the non-UV irradiation of PVAc/TiO_2 composite membrane sample at 5% TiO_2 loading (i.e., no photocatalytic activity) to observe any distinguish changes in materials phase structure, Figure S7C in the Supporting Information. It can be seen that there are no remarkable changes in the FTIR range 1780−3650 cm^{-1} for samples irradiated with and without UV light (Figure S7 in the Supporting Information). The transmission bands at 1740 cm^{-1} (C═O) after UV irradiated samples sharply decreased compared with the non-UV irradiated sample. However, the IR band (C═O) of polymeric fiber samples decorated with TiO_2 NPs remains sharper and stronger than the polymeric fiber with absence of TiO_2 after exposure to UV light, attributing that no distinguishable changes on IR bands after exposure to UV light were observed (see above). This indicated that no phase structure changes was detected using UV photodegrdation in the absence and present of TiO_2-decorated on polymeric substrate.[3]

It was evident that TiO_2 NPs immobilized onto and around spinning nanofibers practically do not lose their photodegradation performance compared to that of TiO_2 NPs themselves.[34] It is important to point out that the demonstrated composite membranes have not been fully optimized for possible industrial applications. It is conceivable that with the addition or incorporation of antimicrobial nanoparticles (e.g., metallic silver and silver oxides)[27] onto the surface of AJS membrane mat and with further reduction of fiber diameter, photocatalytic efficiency can be fully optimized for real industrial application.

4. CONCLUSION AND FUTURE ASPECTS

Hydrophilic photocatalyst TiO_2/PVAc composite nanofiberous membrane mats have been successfully manufactured for the first time using cost-effective air jet spinning strategy. The AJS was designed to process a composite membrane that would be immobilizing active catalyst TiO_2 NPs with a large amount in a short time. SEM micrographs of AJS pristine and composite nanofibrous mats results revealed beadless, nanoscaled fibrous structures formed under controlled conditions. High porosity (>90.%), interconnected pores and large surface area could be attained effortlessly by this accessible technique. TiO_2 NPs (5 wt %) are homogeneously distributed and well-embedded onto and around spinning fibers without aggregation because of the NPs fluctuation and presence of a kinetic energy throughout the process. The thermal stability and crystallinity of PVAc as well as the interfacial bonding between the NPs and as-spun fibers are improved by addition of the TiO_2 NPs. In addition, compared to the most common existing techniques for nanoscale fibers fabrication, the newly developed AJS techniques has some extra advantages where nonwoven webs can be applied directly to any substrate without applying high electric voltage, as in electrospinning. Because AJS is more mobile, metallic, and nonmetallic target could be easily coated with nanofibers.

This study could provide deep understanding and valuable scientific fundamentals for the fabrication of new photocatalyst composite membrane mats. The obtained results of photodegradation test are consistent with the reported literature data. Development of this type of effective photocatalysts is a breakthrough in industrial-scale utilization of water treatment to address the environmental needs. It is our belief that AJS will be one of the most effective and powerful tools for fabrication of high performance membrane materials with broad range of

DOI: 10.1021/acsami.5b01418
ACS Appl. Mater. Interfaces 2015, 7, 13329−13341

applications in multidisciplinary areas such as water treatment and chemically/biologically protective clothing. We expect that this technique, if integrated with computer aided design and manufacturing (CAD/CAM) processes to allow air jet spun fiber mat to be spun onto a commercial water filter media using the digitized form, will allow for the fabrication of more efficient photocatalysts and high flux ultrafiltration membranes.

■ ASSOCIATED CONTENT

Supporting Information

Specification of commercial pure titanium grade 2, SEM morphology observation of as-received TiO_2 NPs, optical 2D image of AJS system designed in our laboratory, optical absorption of methylene blue, SEM photographs of electrospun PVAc pristine fibers, obtical 2D images of AJS collected mat, and AJS deposition membrane fiber mat onto different target, additional SEM images of composite nanofibers, and FTIR spectra. The Supporting Information is available free of charge on the ACS Publications website at DOI: 10.1021/acsami.5b01418.

■ AUTHOR INFORMATION

Corresponding Authors

*E-mail: abda_55@jbnu.ac.kr. Tel: +20965330640.
*E-mail: abdel.makhlouf@utrgv.edu. Tel: 1 (956)-665-8956.

Notes

The authors declare no competing financial interest.

■ ACKNOWLEDGMENTS

The authors would like to extend their sincere appreciation to the Deanship of Scientific Research at King Saud University for its funding of this Research Group No. (RG 1435-001).

■ REFERENCES

(1) Tahir, M.; Amin, N. S. Indium-Doped TiO_2 Nanoparticles for Photocatalytic CO_2 Reduction with H_2O Vapors to CH_4. *Appl. Catal., B* **2015**, *162*, 98−109.
(2) Wang, P.; Li, D.; Chen, J.; Zhang, X.; Xian, J.; Yang, X.; Zheng, X.; Li, X.; Shao, Y. A Novel and Green Method to Synthesize CdSe Quantum Dots-Modified TiO_2 and its Enhanced Visible Light Photocatalytic Activity. *Appl. Catal., B* **2014**, *160−161*, 217−226.
(3) Lee, J. A.; Krogman, K. C.; Ma, M.; Hill, R. M.; Hammond, P. T.; Rutledge, G. C. Highly Reactive Multilayer-Assembled TiO_2 Coating on Electrospun Polymer Nanofibers. *Adv. Mater.* **2009**, *21*, 1252−1256.
(4) Liang, H. W.; Zhang, W. J.; Ma, Y. N.; Cao, X.; Guan, Q. F.; Xu, W. P.; Yu, S. H. Highly Active Carbonaceous Nanofibers: A Versatile Scaffold for Constructing Multifunctional Free-Standing Membranes. *ACS Nano* **2011**, *5*, 8148−8161.
(5) Monteiro, R. A. R.; Miranda, S. M.; Vilar, V. J. P.; Pastrana-Martínez, L. M.; Tavares, P. B.; Boaventura, R. A. R.; Faria, J. L.; Pinto, E.; Silva, A. M. T. N-Modified TiO_2 Photocatalytic Activity Towards Diphenhydramine Degradation and Escherichia Coli Inactivation in Aqueous Solutions. *Appl. Catal., B* **2015**, *162*, 66−74.
(6) Obata, K.; Kishishita, K.; Okemoto, A.; Taniya, K.; Ichihashi, Y.; Nishiyama, S. Photocatalytic Decomposition of NH_3 over TiO_2 Catalysts Doped with Fe. *Appl. Catal., B* **2014**, *160−161*, 200−203.
(7) Zhao, S.; Ren, J.; Wang, Y.; Zhang, J. Electric Field Processing to Control The Structure of Titanium Oxide/Sulfonated Poly (Ether Ether Ketone) Hybrid Proton Exchange Membranes. *J. Membr. Sci.* **2013**, *437*, 65−71.
(8) Reijnders, L. Hazard Reduction for The Application of Titania Nanoparticles in Environmental Technology. *J. Hazard Mater.* **2008**, *152*, 440−445.
(9) Linsebigler, A. L.; Lu, G.; Yates, J. T. Photocatalysis on TiO_2 Surfaces: Principles, Mechanisms, and Selected Results. *Chem. Rev.* **1995**, *95*, 735−758.
(10) Schmidt, H.; Naumann, M.; Müller, T. S.; Akarsu, M. Application of Spray Techniques for New Photocatalytic Gradient Coatings on Plastics. *Thin Solid Films* **2006**, *502*, 132−137.
(11) Hojamberdiev, M.; Prasad, R. M.; Morita, K.; Zhu, Y.; Schiavon, M. A.; Gurlo, A.; Riedel, R. Template-free Synthesis of Polymer-Derived Mesoporous SiOC/TiO_2 and SiOC/N-doped TiO_2 Ceramic Composites For Application in the Removal of Organic Dyes from Contaminated Water. *Appl. Catal., B* **2012**, *115−116*, 303−313.
(12) Lee, C.-S.; Kim, J.; Son, J. Y.; Choi, W.; Kim, H., Photocatalytic Functional Coatings of TiO_2 Thin Films on Polymer Substrate by Plasma Enhanced Atomic Layer Deposition. *Appl. Catal., B, 91*, 628−633.
(13) Lim, S. K.; Lee, S.-K.; Hwang, S.-H.; Kim, H. Photocatalytic Deposition of Silver Nanoparticles onto Organic/Inorganic Composite Nanofibers. *Macromol. Mater. Eng.* **2006**, *291*, 1265−1270.
(14) Benavides, R. E.; Jana, S. C.; Reneker, D. H. Nanofibers from Scalable Gas Jet Process. *ACS Macro Lett.* **2012**, *1*, 1032−1036.
(15) Abdal-hay, A.; Barakat, N. A. M.; Lim, J. K. Novel Technique for Polymeric Nanofibers Preparation: Air Jet Spinning. *Sci. Adv. Mater.* **2012**, *4*, 1−8.
(16) Abdal-hay, A.; Vanegas, P.; Lim, J. K. Air Jet Spray of Nylon 6 Membrane Structures for Bone Tissue Engineering. *Mater. Lett.* **2014**, *125*, 51−55.
(17) Abdal-hay, A.; Hamdy, A. S.; Abdellah, M. Y.; Lim, J. In Vitro Bioactivity of Implantable Ti Materials Coated with PVAc Membrane Layer. *Mater. Lett.* **2014**, *126*, 267−270.
(18) Vargha, V.; Truter, P. Biodegradable Polymers by Reactive Blending Trans-Esterification of Thermoplastic Starch with Poly(Vinyl Acetate) And Poly(Vinyl Acetate-Co-Butyl Acrylate). *Eur. Polym. J.* **2005**, *41*, 715−726.
(19) Sivalingam, G. Blends of poly(caprolactone) and poly(vinyl acetate): Mechanical Properties and Thermal Degradation. *Polym. Degrad. Stab.* **2004**, *84*, 345−351.
(20) Abdal-hay, A.; Dewidar, M.; Lim, J. K. Biocorrosion Behavior and Cell Viability of Adhesive Polymer Coated Magnesium Based Alloys for Medical Implants. *Appl. Surf. Sci.* **2012**, *261*, 536−546.
(21) Xu, Z.-l.; Yu, L.-y.; Han, L.-f. Polymer-Nanoinorganic Particles Composite Membranes: A Brief Overview. *Front. Chem. Eng. China* **2009**, *3*, 318−329.
(22) Abdal-hay, A.; Mousa, H. M.; Khan, A.; Vanegas, P.; Lim, J. H. TiO_2 Nanorods Coated onto Nylon 6 Nanofibers Using Hydrothermal Treatment with Improved Mechanical Properties. *Colloids Surf., A* **2014**, *457*, 275−281.
(23) Fu, G. D.; Xu, L. Q.; Yao, F.; Zhang, K.; Wang, X. F.; Zhu, M. F.; Nie, S. Z. Smart Nanofibers From Combined Living Radical Polymerization, "Click Chemistry", and Electrospinning. *ACS Appl. Mater. Interfaces* **2009**, *1*, 239−243.
(24) Lee, J. B.; Jeong, S. I.; Bae, M. S.; Yang, D. H.; Heo, D. N.; Kim, C. H.; Alsberg, E.; Kwon, I. K. Highly Porous Electrospun Nanofibers Enhanced by Ultrasonication for Improved Cellular Infiltration. *Tissue Eng., Part A* **2011**, *17*, 2695−2702.
(25) Jana, S.; Cooper, A.; Ohuchi, F.; Zhang, M. Uniaxially Aligned Nanofibrous Cylinders by Electrospinning. *ACS Appl. Mater. Interfaces* **2012**, *4*, 4817−4824.
(26) Abdal-hay, A.; Sheikh, F. A.; Lim, J. K. Air Jet Spinning of Hydroxyapatite/Poly(Lactic Acid) Hybrid Nanocomposite Membrane Mats for Bone Tissue Engineering. *Colloids Surf., B* **2013**, *102*, 635−643.
(27) Barhate, R. S.; Ramakrishna, S. Nanofibrous filtering media: Filtration problems and solutions from tiny materials. *J. Membr. Sci.* **2007**, *296*, 1−8.
(28) Fang, J.; Niu, H.; Lin, T.; Wang, X. Applications of Electrospun Nanofibers. *Chin. Sci. Bull.* **2008**, *53* (15), 2265−2286.
(29) Abdal-hay, A.; Oh, Y. S.; Yousef, A.; Pant, H. R.; Vanegas, P.; Lim, J. K. In Vitro Deposition of Ca-P Nanoparticles on Air Jet

DOI: 10.1021/acsami.5b01418
ACS Appl. Mater. Interfaces 2015, 7, 13329−13341

Spinning Nylon 6 Nanofibers Scaffold for Bone Tissue Engineering. *Appl. Surf. Sci.* **2014**, *307*, 69−76.
(30) François, S.; Chakfé, N.; Durand, B.; Laroche, G. A Poly(L-Lactic Acid) Nanofibre Mesh Scaffold for Endothelial Cells on Vascular Prostheses. *Acta Biomater.* **2009**, *5*, 2418−2428.
(31) Yoon, K.; Kim, K.; Wang, X.; Fang, D.; Hsiao, B. S.; Chu, B. High Flux Ultrafiltration Membranes Based on Electrospun Nanofibrous Pan Scaffolds and Chitosan Coating. *Polym.* **2006**, *47*, 2434−2441.
(32) Pant, H. R.; Bajgai, M. P.; Nam, K. T.; Seo, Y. A.; Pandeya, D. R.; Hong, S. T.; Kim, H. Y. Electrospun Nylon-6 Spider-Net Like Nanofiber Mat Containing TiO_2 Nanoparticles: A Multifunctional Nanocomposite Textile Material. *J. Hazard Mater.* **2011**, *185*, 124−130.
(33) Pant, H. R.; Pant, B.; Pokharel, P.; Kim, H. J.; Tijing, L. D.; Park, C. H.; Lee, D. S.; Kim, H. Y.; Kim, C. S. Photocatalytic TiO_2-RGO/Nylon-6 Spider-Wave-Like Nano-Nets via Electrospinning and Hydrothermal Treatment. *J. Membr. Sci.* **2013**, *429*, 225−234.
(34) Pant, H. R.; Pandeya, D. R.; Nam, K. T.; Baek, W. I.; Hong, S. T.; Kim, H. Y. Photocatalytic and Antibacterial Properties of a TiO_2/Nylon-6 Electrospun Nanocomposite Mat Containing Silver Nanoparticles. *J. Hazard Mater.* **2011**, *189*, 465−71.
(35) Paulsen, F. G.; Shojaie, S. S.; Krantz, W. B. Effect of Evaporation Step On Macrovoid Formation In Wet-Cast Polymeric Membranes. *J. Membr. Sci.* **1994**, *91*, 265−282.
(36) Tutak, W.; Sarkar, S.; Lin-Gibson, S.; Farooque, T. M.; Jyotsnendu, G.; Wang, D.; Kohn, J.; Bolikal, D.; Simon, C. G., Jr. The Support of Bone Marrow Stromal Cell Differentiation by Airbrushed Nanofiber Scaffolds. *Biomaterials* **2013**, *34*, 2389−2398.
(37) Ahmad, J.; Hägg, M.-B. Preparation and Characterization of Polyvinyl Acetate/Zeolite 4A Mixed Matrix Membrane for Gas Separation. *J. Membr. Sci.* **2013**, *427*, 73−84.
(38) Grassie, N.; McLean, I. F.; McNeill, I. C. Thermal Degradation of Vinyl Chloride-Vinyl Acetate Copolymers- i. Bulk Degradation Studies by Thermal Volatilization Analysis. *Eur. Polym. J.* **1970**, *6*, 679−686.
(39) Troitskii, B. B.; Razuvaev, G. A.; Khokhlova, L. V.; Bortnikov, G. N. On the Mechanism of the Thermal Degradation of Polyvinyl Acetate. *J. Appl. Polym. Sci.: Appl. Polym. Symp.* **1973**, *42*, 1363−1375.
(40) Sivalingam, G.; Karthik, R.; Madras, G. Effect of Metal Oxides on Thermal Degradation of Poly(vinyl acetate) and Poly(vinyl chloride) and Their Blends. *Ind. Eng. Chem. Res.* **2003**, *42* (16), 3647−3653.
(41) Abdal-hay, A.; Pant, H. R.; Lim, J. K. Super-Hydrophilic Electrospun Nylon-6/Hydroxyapatite Membrane for Bone Tissue Engineering. *Eur. Polym. J.* **2013**, *49*, 1314−1321.
(42) Ahmad, J.; Hågg, M. B. Polyvinyl Acetate/Titanium Dioxide Nanocomposite Membranes for Gas Separation. *J. Membr. Sci.* **2013**, *445*, 200−210.
(43) Mack, J. J.; Viculis, L. M.; Ali, A.; Luoh, R.; Yang, G.; Hahn, H. T.; Ko, F. K.; Kaner, R. B. Graphite Nanoplatelet Reinforcement of Electrospun Polyacrylonitrile Nanofibers. *Adv. Mater.* **2005**, *17*, 77−80.
(44) Shah, M. S. A. S.; Nag, M.; Kalagara, T.; Singh, S.; Manorama, S. V. Silver on PEG-PU-TiO_2 Polymer Nanocomposite Films: An Excellent System for Antibacterial Applications. *Chem. Mater.* **2008**, *20*, 2455−2460.
(45) Kong, H.; Song, J.; Jang, J. Photocatalytic Antibacterial Capabilities of TiO_2-Biocidal Polymer Nanocomposites Synthesized by a Surface-Initiated Photopolymerization. *Environ. Sci. Technol.* **2010**, *44*, 5672−5676.
(46) Sohn, B.-H.; Kim, T.-H.; Char, K. Process-Dependent Photocatalytic Properties of Polymer Thin Films Containing TiO_2 Nanoparticles: Dip vs Spin Self-Assembly Methods. *Langmuir* **2002**, *18*, 7770−7772.
(47) Dhananjeyan, M. R.; Kiwi, J.; Thampi, K. R. Photocatalytic Performance of TiO_2 and Fe_2O_3 Immobilized on Derivatized Polymer Films for Mineralisation of Pollutants. *Chem. Commun.* **2000**, *15*, 1443−1444.
(48) Dong, H.; Fey, E.; Gandelman, A.; Jones, W. E. Synthesis and Assembly of Metal Nanoparticles on Electrospun Poly(4-vinylpyridine) Fibers and Poly(4-vinylpyridine) Composite Fibers. *Chem. Mater.* **2006**, *18*, 2008−2011.
(49) Yang, Y.; Zhang, H.; Wang, P.; Zheng, Q.; Li, J. The influence of Nano-Sized TiO_2 Fillers on The Morphologies and Properties of Psf Uf Membrane. *J. Membr. Sci.* **2007**, *288*, 231−238.
(50) Wang, B.; Chen, Z.; Zhang, J.; Cao, J.; Wang, S.; Tian, Q.; Gao, M.; Xu, Q. Fabrication of PVA/Graphene Oxide/TiO_2 Composite Nanofibers Through Electrospinning and Interface Sol−Gel Reaction: Effect of Graphene Oxide on PVA Nanofibers and Growth of TiO_2. *Colloids Surf., A* **2014**, *457*, 318−325.
(51) Wong, S.-C.; Baji, A.; Leng, S. Effect of Fiber Diameter on Tensile Properties of Electrospun Poly(ε-caprolactone). *Polymer* **2008**, *49* (21), 4713−4722.
(52) Podgórski, A.; Bałazy, A.; Gradoń, L. Application of Nanofibers to Improve the Filtration Efficiency of the Most Penetrating Aerosol Particles in Fibrous Filters. *Chem. Eng. Sci.* **2006**, *61*, 6804−6815.
(53) Abdal-hay, A.; Hwang, M.-G.; Lim, J. In Vitro Bioactivity of Titanium Implants Coated with Bicomponent Hybrid Biodegradable Polymers. *J. Sol−Gel Sci. Technol.* **2012**, *64*, 756−764.
(54) Lu, X.; Wang, Y.-b.; Liu, Y.-r.; Wang, J.-x.; Qu, S.-x.; Feng, B.; Weng, J. Preparation of HA/Chitosan Composite Coatings on Alkali Treated Titanium Surfaces Through Sol-Gel Techniques. *Mater. Lett.* **2007**, *61*, 3970−3973.
(55) Abdal-Hay, A.; Hamdy, A. S.; Khalil, K. A.; Lim, J. H. A Novel Simple one-Step Air Jet Spinning Approach for Deposition of Poly(Vinyl Acetate)/Hydroxyapatite Composite Nanofibers on Ti Implants. *Mater. Sci. Eng., C* **2015**, *49*, 681−690.
(56) Rezwan, K.; Chen, Q. Z.; Blaker, J. J.; Boccaccini, A. R. Biodegradable and Bioactive Porous Polymer/Inorganic Composite Scaffolds for Bone Tissue Engineering. *Biomaterials* **2006**, *27*, 3413−3431.

DOI: 10.1021/acsami.5b01418
ACS Appl. Mater. Interfaces 2015, 7, 13329−13341